Applied Mathematics and Computation 364 (2020) 124670

Contents lists available at ScienceDirect

Applied Mathematics and Computation

journal homepage: www.elsevier.com/locate/amc

Random walk methods for Monte Carlo simulations of Brownian diffusion on a sphere

A. Novikov [a], D. Kuzmin [b,*], O. Ahmadi [b]

[a] Department of Mathematics, Penn State University, University Park, PA 16802, USA
[b] Institute of Applied Mathematics (LS III), TU Dortmund University, Vogelpothsweg 87, Dortmund D-44227, Germany

ARTICLE INFO

Article history:
Received 17 February 2019
Revised 11 July 2019
Accepted 12 August 2019
Available online 27 August 2019

Keywords:
Brownian diffusion on a sphere
Laplace–Beltrami operator
Orientation probability density
Lagrangian modeling
Random walk

ABSTRACT

This paper is focused on efficient Monte Carlo simulations of Brownian diffusion effects in particle-based numerical methods for solving transport equations on a sphere (or a circle). Using the heat equation as a model problem, random walks are designed to emulate the action of the Laplace–Beltrami operator without evolving or reconstructing the probability density function. The intensity of perturbations is fitted to the value of the rotary diffusion coefficient in the deterministic model. Simplified forms of Brownian motion generators are derived for rotated reference frames, and several practical approaches to generating random walks on a sphere are discussed. The alternatives considered in this work include projections of Cartesian random walks, as well as polar random walks on the tangential plane. In addition, we explore the possibility of using look-up tables for the exact cumulative probability of perturbations. Numerical studies are performed to assess the practical utility of the methods under investigation.

1. Introduction

The need for efficient numerical modeling of Brownian diffusion effects on a unit sphere arises, e.g., in fiber suspension flow models based on the Fokker–Planck equation for the orientation probability density [1,2]. This equation is derived from the Jeffery equation [3] for a single ellipsoid using (possibly anisotropic) rotary diffusion terms to model fiber interactions in concentrated suspension models. Direct numerical solution of the Fokker–Plank equation incurs exorbitant computational cost since the probability density function of fiber orientation depends on two orientation angles in addition to the space and time variables. Therefore, Eulerian models implemented in most industrial and research codes produce just a few even-order moments of the probability density function (so-called orientation tensors) [1].

Lagrangian methods for simulation of disperse two-phase flows are based on solving individual equations of motion for each particle or fiber [4–7]. Whereas the cost of evolving a single fiber is negligible compared to that of solving a multi-dimensional PDE, the large number of fibers that are required for accurate prediction of local orientation states can make Lagrangian simulations far more expensive than Eulerian tensor evolution models. Additionally, the numerical treatment of Brownian diffusion effects is more difficult in the Lagrangian framework. Since diffusive fluxes describe changes of the probability density function due to random microscopic motions, stochastic perturbations must be applied to the spatial

* Corresponding author.
E-mail addresses: anovikov@math.psu.edu (A. Novikov), kuzmin@math.uni-dortmund.de (D. Kuzmin), omid.ahmadi@math.tu-dortmund.de (O. Ahmadi).

https://doi.org/10.1016/j.amc.2019.124670
0096-3003/

coordinates and/or orientation angles of moving fibers to emulate the impact of these fine-scale effects on the trajectory and orientation of Lagrangian particles/fibers [6,7].

In this paper, we focus on the derivation and numerical study of random walk methods for the heat equation on a unit sphere. The ability to obtain accurate solutions to this model problem in an efficient manner is a prerequisite for achieving high performance when it comes to Lagrangian simulations involving convective transport of fibers in the 3D space, deterministic changes of their orientation caused by velocity gradients, and a two-way coupling with the generalized Navier–Stokes equations for the velocity field.

In Sections 2 and 3, we introduce deterministic and stochastic approaches to numerical simulation of fiber orientation dynamics in the context of the spherical heat equation. Section 4 presents stochastic PDE analysis which provides theoretical foundations for generating Brownian motions and random walks. In Section 5, we focus on practical algorithms for generation of random numbers corresponding to given values of the rotary diffusion coefficient. Some of the methods to be presented are based on projections of standard Cartesian random walks. Others rotate Brownian fibers by adding perturbations to the polar coordinates in the tangential plane. In the method proposed by Chen and Yu [8], angular perturbations are generated using cumulative probability derived from an approximate solution of the spherical heat equation. This approach produces accurate results as long as the time step is sufficiently small. In computations with larger time steps, we use a tabulated numerical approximation to the cumulative distribution function given by the exact solution of the spherical heat equation. After presenting the new algorithms and discussing their properties, we perform numerical studies and compare the results obtained with different methods.

2. Deterministic modeling of Brownian diffusion

The orientation of a rigid rod-like fiber in $d = 2, 3$ space dimensions is characterized by a point $\mathbf{p} \in \mathbb{S}^{d-1}$ on the unit sphere $\mathbb{S}^{d-1} := \{\mathbf{p} \in \mathbb{R}^d : \|\mathbf{p}\| = 1\}$, where $\|\cdot\|$ is the Euclidean vector norm. Let $f(\mathbf{x}, \mathbf{p}, t)$ denote the probability that a fiber occupying the space location $\mathbf{x} \in \mathbb{R}^d$ has orientation $\mathbf{p} \in \mathbb{S}^{d-1}$ at time $t \in \mathbb{R}_+$. In the absence of spatial gradients, the Fokker–Planck equation for the probability density function $f = f(\mathbf{p}, t)$ of a concentrated fiber suspension reduces to the spherical heat equation

$$\frac{\partial f}{\partial t} = D\Delta_p f \quad \text{on } \mathbb{S}^2, \tag{1}$$

where $D > 0$ is a rotary diffusion coefficient and Δ_p is the Laplace–Beltrami operator, i.e., the tangential divergence of the tangential gradient.

Written in spherical coordinates, each three-dimensional orientation state $\mathbf{p} \in \mathbb{S}^2$ becomes a function of two orientation angles. We have

$$\mathbf{p} = \begin{pmatrix} p_1 \\ p_2 \\ p_3 \end{pmatrix} = \begin{pmatrix} \sin\theta\cos\varphi \\ \sin\theta\sin\varphi \\ \cos\theta \end{pmatrix}, \quad \varphi \in [0, 2\pi), \quad \theta \in [0, \pi]. \tag{2}$$

Using the fact that $r := \|\mathbf{p}\| = 1$ for $\mathbf{p} \in \mathbb{S}^2$, we restrict the Laplace operator

$$\Delta = \frac{1}{r^2}\frac{\partial}{\partial r}\left(r^2\frac{\partial}{\partial r}\right) + \frac{1}{r^2\sin\theta}\frac{\partial}{\partial\theta}\left(\sin\theta\frac{\partial}{\partial\theta}\right) + \frac{1}{r^2\sin^2\theta}\frac{\partial^2}{\partial\varphi^2} \tag{3}$$

to the unit sphere and obtain the formula for Δ_p in spherical coordinates

$$\Delta_p = \frac{1}{\sin\theta}\frac{\partial}{\partial\theta}\left(\sin\theta\frac{\partial}{\partial\theta}\right) + \frac{1}{\sin^2\theta}\frac{\partial^2}{\partial\varphi^2}. \tag{4}$$

In contrast to the heat equation in $\mathbb{R}^3$, its spherical counterpart (1) cannot be readily solved by convolving an arbitrary initial condition with a Gaussian kernel. However, if the initial condition is given by the δ distribution

$$f(\mathbf{p}(\theta, \varphi), 0) = \delta(\mathbf{p}_0), \quad \mathbf{p}_0 \in \mathbb{S}^2 \tag{5}$$

corresponding to the case of full alignment (i.e., of all fibers having the same orientation $\mathbf{p}_0$ at $t = 0$), the exact solution of the initial value problem for the spherical heat equation can be derived using the change of variables

$$(x_1, x_2, x_3) \mapsto (\hat{x}_1, \hat{x}_2, \hat{x}_3), \quad (\theta, \varphi) \mapsto (\hat{\theta}, \hat{\varphi})$$

such that the unit vector $\hat{e}_3 = (0, 0, 1)^T$ of the rotated Cartesian coordinate system coincides with the direction $\mathbf{p}_0$ of initial alignment (see Fig. 1). In this reference frame, the initial condition (5) is independent of the polar angle $\hat{\varphi}$ and so is the probability density $f = f(\hat{x}_3, t)$, $\hat{x}_3 = \cos\hat{\theta}$ for $t > 0$. It follows that:

$$\hat{\Delta}_p f = \frac{\partial}{\partial\hat{x}_3}\left((1 - \hat{x}_3^2)\frac{\partial f}{\partial\hat{x}_3}\right) \tag{6}$$

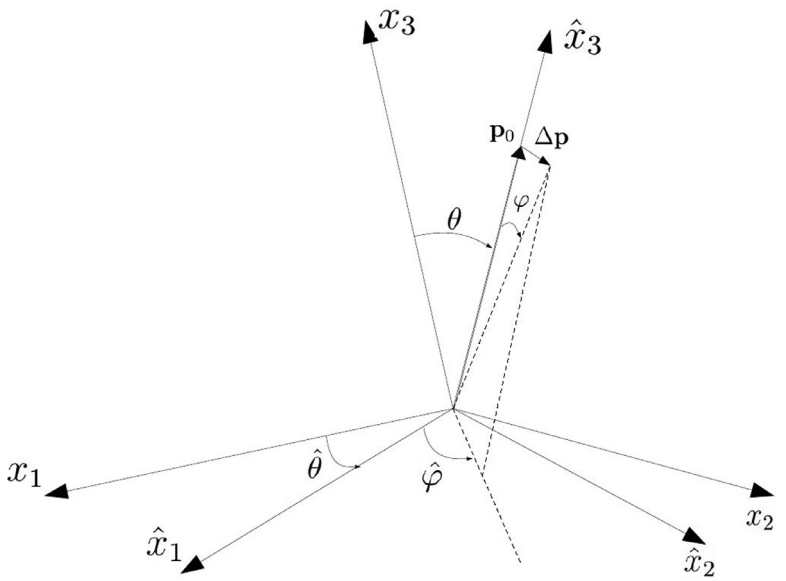

Fig. 1. Coordinate system in which $\mathbf{p}_0 = (0, 0, 1)^T$, cf. [8].

and, therefore, the initial value problem at hand simplifies to

$$\frac{\partial f}{\partial t} = D\frac{\partial}{\partial \hat{x}_3}\left((1-\hat{x}_3^2)\frac{\partial f}{\partial \hat{x}_3}\right), \quad (\hat{x}_3, t) \in [-1, 1] \times \mathbb{R}_+, \tag{7}$$

$$f(\hat{x}_3, 0) = \delta(1), \quad \hat{x}_3 \in [-1, 1]. \tag{8}$$

The exact solution of problem (7), (8) is given by [8,9]

$$f(\hat{x}_3, t) = \sum_{n=0}^{\infty} \frac{2n+1}{2} \exp\left(-n(n+1)Dt\right) P_n(\hat{x}_3), \tag{9}$$

where P_n is the nth Legendre polynomial. In what follows, we will use this formula to generate look-up tables for random walks on $\mathbb{S}^2$.

In practice, the evaluation of $f(\hat{x}_3, t)$ defined by (9) requires approximation of the infinite series by a partial sum. The number of terms that provide an accurate description of f may be significant. Orientation tensors representing the first even-order moments of the probability density distribution can be calculated exactly using just a few terms (see Section 6 for details).

If the time interval is restricted to $[0, \Delta t]$ such that $D\Delta t \ll 1$, then $f(\hat{x}_3, t)$ can be nonvanishing only for small values of the azimuthal angle $\hat{\theta} = \arccos \hat{x}_3$ since $f(\hat{x}_3, 0) = 0$ for $\hat{\theta} > 0$. Following Chen and Wu [8], we use the small angle approximation $\sin\hat{\theta} \approx \hat{\theta}$ and consider the simplified problem

$$\frac{\partial f(\cos\hat{\theta}, t)}{\partial t} = \frac{D}{\hat{\theta}}\frac{\partial}{\partial \hat{\theta}}\left(\hat{\theta}\frac{\partial f(\cos\hat{\theta}, t)}{\partial \hat{\theta}}\right), \quad (\hat{\theta}, t) \in [0, \pi] \times \mathbb{R}_+. \tag{10}$$

The exact solution corresponding to the initial δ distribution reads [8]

$$f(\cos\hat{\theta}, t) = \frac{1}{4\pi Dt}\exp\left(-\frac{\hat{\theta}^2}{4Dt}\right), \quad t \in (0, \Delta t]. \tag{11}$$

This approximation to (9) can be evaluated efficiently and produces accurate results as long as $D\Delta t \ll 1$, as assumed in the derivation of (10).

For general initial conditions, no closed-form analytical solutions of (1) are known but numerical solutions of arbitrary high precision can be obtained using Galerkin methods based on approximations of the form

$$f_M(\mathbf{p}, t) = \sum_{j=1}^{M} c_j(t)\psi_j(\mathbf{p}), \tag{12}$$

where $c_j(t)$ is the time-dependent degree of freedom associated with the basis function $\psi_j(\mathbf{p})$. For example, spherical harmonics or linear finite elements a cubed sphere grid can be used to discretize the spherical heat equation in this manner.

However, extensions of such numerical methods to the general Fokker–Planck equation for a space-dependent probability distribution $f(\mathbf{x}, \mathbf{p}, t)$ would require solution of a three-dimensional evolution equation for each orientation mode $c_j(\mathbf{x}, t)$. We refer to [10,11] for examples of *alternating direction* methods based on this computationally intensive Eulerian approach to numerical treatment of the Fokker–Planck equation. In the remainder of this article, we focus on approaches in which orientation states are determined using Monte Carlo simulations of individual fibers.

3. Stochastic modeling of Brownian diffusion

Instead of evolving the probability density function $f(\mathbf{x}, \mathbf{p}, t)$ of a fiber suspension, the centers of mass $\mathbf{x}_m(t)$ and orientation vectors $\mathbf{p}_m(t)$ of N_f representative fibers are evolved in Lagrangian methods [4–6,8]. Brownian diffusion effects are taken into account by adding random perturbations to $\mathbf{x}_i(t)$ and/or $\mathbf{p}_i(t)$. Restricting our attention to Brownian diffusion on the unit sphere $\mathbb{S}^2$, we consider algorithms that lead to updates of the form

$$\mathbf{p}_m^{n+1} = \mathbf{p}_m^n + \Delta\mathbf{p}_m^n, \quad m = 1, \ldots, N_f, \quad n = 0, 1, \ldots, \tag{13}$$

where $\Delta\mathbf{p}_m$ is a random perturbation such that $\mathbf{p}_m + \Delta\mathbf{p}_m \in \mathbb{S}^2$ for $\mathbf{p}_m \in \mathbb{S}^2$.

For sufficiently large values of N_f and n, the probability that some fiber will have orientation $\mathbf{p} \in \mathbb{S}^2$ after n steps can be approximated by

$$\tilde{f}^n(\mathbf{p}) = \frac{1}{N_f} \sum_{m=1}^{N_f} \delta(\mathbf{p} - \mathbf{p}_m^n). \tag{14}$$

Since we are interested in solving the spherical heat equation, this probability distribution should correspond to an approximate solution of (1) at the time instant $t^n = n\Delta t$, where Δt is a constant time step size. To that end, the intensity of random perturbations should be defined so as to obtain the correct mean squared displacement or correct cumulative probability.

The following approaches to Monte Carlo simulations based on the addition of perturbations $\Delta\mathbf{p}^n$ to orientation vectors $\mathbf{p} \in \mathbb{S}^2$ can be envisaged:

- Construct $\Delta\mathbf{p} = (\Delta p_1, \Delta p_2, \Delta p_3)^T$ as in the standard random walk method for Brownian diffusion in $\mathbb{R}^3$ and project $\mathbf{p} + \Delta\mathbf{p}$ onto $\mathbb{S}^2$;
- Perform standard random walk on the tangential plane orthogonal to the orientation vector $\mathbf{p} \in \mathbb{S}^2$ and project $\mathbf{p} + \Delta\mathbf{p}$ onto $\mathbb{S}^2$;
- Perform random walk on $\mathbb{S}^2$ using the fiber-aligned reference frame $\{\hat{e}_1, \hat{e}_2, \hat{e}_3\}$ in which $\hat{\mathbf{p}} = (0, 0, 1)^T$ is the North Pole;

The first approach is described in Section 5.2. It was used, e.g., by Moosaie and Manhart [6] for direct Monte Carlo simulations of fiber suspension flows. The third approach was adopted in the work of Chen and Wu [8] who used (11) to construct an approximate inverse of the cumulative probability function and calculate angular perturbations (see Section 5.3). Note that the use of a reference frame aligned with the orientation vector $\mathbf{p}$ is consistent with the assumption of a δ distribution for the unperturbed initial state.

In contrast to the first two approaches, which exploit the knowledge of analytical solutions, the third one requires direct construction of a Brownian motion associated with the Laplace–Beltrami operator Δ_p. We accomplish this task in the next section using some basic tools of probability theory and stochastic PDE analysis. Practical implementation of different random walks based on the above three approaches is discussed in Section 5. Projection-based algorithms involving random walks on $\mathbb{S}^3$ be found in [12,13].

4. Brownian motion

We use uppercase letters for random variables and lowercase letters for their deterministic counterparts. For example, θ is a deterministic angle, whereas Θ is a random angle. The value of Θ is a set of numbers, the distribution of which depends on random events such as a coin toss. Similarly, $b(t)$, $t \in [0, \infty)$ is a continuous trajectory, whereas a one-dimensional standard Brownian motion $B(t)$, $t \in [0, \infty)$ is a *stochastic process*, that, is a set of continuous trajectories such that for any fixed t and s, the distributions of random variables $B(t+s) - B(t)$ and $B(t)$ are independent, Gaussian (i.e., normal) with expected value

$$\mathbb{E}[(B(t+s) - B(t))] = \mathbb{E}[B(t)] = 0,$$

and variance

$$\mathrm{Var}[B(t+s) - B(s)] = \mathbb{E}[(B(t+s) - B(t))^2] = s, \quad \mathrm{Var}[B(t)] = t.$$

4.1. Brownian motion and the Laplacian

We say that the Laplacian $Lf = D\Delta f$ is the generator of a (rescaled) Brownian motion for the following reason. The solution of the initial value problem

$$\frac{\partial f}{\partial t}(\mathbf{x}, t) = D\Delta f(\mathbf{x}, t), \quad (\mathbf{x}, t) \in \mathbb{R}^d \times \mathbb{R}_+, \tag{15}$$

$$f(\mathbf{x}, 0) = \delta(\mathbf{0}) \tag{16}$$

is the probability density of a (rescaled) Brownian particle $X(t)$ that starts at the origin at $t = 0$: $X(0) = 0$. This density corresponds to the Gaussian distribution

$$f(\mathbf{x}, t) = \left(\frac{1}{2\sqrt{Dt\pi}}\right)^d e^{\frac{-\|\mathbf{x}\|^2}{4Dt}} \tag{17}$$

and has the variance [7]

$$\sigma_d^2(t) = \int_{\mathbb{R}^d} \|\mathbf{x}\|^2 f(\mathbf{x}, t)\, \mathrm{d}\mathbf{x} = 2dDt. \tag{18}$$

For any $t > 0$, the position of a Brownian particle is a (d-dimensional) random variable with mean $\mathbf{0} \in \mathbb{R}^d$ and variance $2Dt\mathbf{I}$, where $\mathbf{I}$ is the identity matrix. The underlying stochastic process is given by

$$X(t) = \sqrt{2D}B(t), \tag{19}$$

where $B(t) = (B_1(t), B_2(t), \ldots, B_d(t))$ contains d copies of independent one-dimensional standard Brownian motions. The term *standard deviation* is frequently used to describe the behavior of the particle. Informally, it characterizes how far the particle may travel from its original position in time t. Formally, the standard deviation is the square root of the trace of the variance. For $X(t)$ defined by (19) the standard deviation is $\sigma_d(t) = \sqrt{2dDt}$.

4.2. Brownian motion and the random walk

Donsker's theorem (also known as the functional central limit theorem) demonstrates rigorously that the one-dimensional Brownian motion $B(t)$ with variance $\sigma^2 t$ is a limit of a wide class of piecewise-linear random trajectories $Y_k(t) \to B(t)$ as $k \to \infty$. Such trajectories $Y_k(t)$ can be constructed using a random walk as follows. Draw countably many independent random variables X_i, $i \in \mathbb{N}$ using the same distribution with mean zero and variance σ^2. The associated random walk is given by

$$S_n = \sum_{i=1}^{n} X_i, \quad n \in \mathbb{N}.$$

For a fixed time-step $\Delta t = 1/k$, define the piecewise-linear random trajectory

$$Y_k(t) = \sqrt{\Delta t}\left(S_{\lfloor t/\Delta t \rfloor} + (t - \lfloor t/\Delta t \rfloor \Delta t) X_{\lfloor t/\Delta t \rfloor + 1}\right),$$

where the floor function $\lfloor t/\Delta \rfloor$ returns the largest integer smaller than $t/\Delta t$. Formally, each random number X_i corresponds to a one-dimensional displacement of a moving particle at a discrete time step Δt. The average distance traveled by the particle per time step in a given space direction is $\sigma\sqrt{\Delta t}$. It follows that the Brownian motion (19) can be generated from i.i.d. (independent, identically distributed) random numbers with mean zero and standard deviation $\sigma = \sqrt{2D}$.

If a distribution of a random number has a finite variance, it can be normalized to be mean-zero. Therefore, Donsker's theorem implies that *any* i.i.d. random numbers with finite variance can be used to approximate a Brownian motion. In view of this fact, the practical choice of such distributions is often dictated by the simplicity of their numerical implementation.

4.3. Brownian motion on a circle

For any standard (mean-zero, variance-one) one-dimensional Brownian motion $B(t)$, a variance-σ^2 Brownian motion on a circle is defined by

$$X(t) = (X_1(t), X_2(t)) = (\cos(\sigma B(t)), \sin(\sigma B(t))).$$

The polar coordinate form of its generator is simply

$$Lf = \frac{\sigma^2}{2}\frac{\partial^2 f}{\partial \varphi^2}. \tag{20}$$

The Cartesian representation is

$$Lf = \frac{\sigma^2}{2}\left(-x_1\frac{\partial f}{\partial x_1} - x_2\frac{\partial f}{\partial x_2} + x_2^2\frac{\partial^2 f}{\partial x_1^2} - 2x_1x_2\frac{\partial^2 f}{\partial x_1 \partial x_2} + x_1^2\frac{\partial^2 f}{\partial x_2^2}\right).$$

Equivalently

$$Lf = \frac{\sigma^2}{2}\left(-x_1\frac{\partial f}{\partial x_1} - x_2\frac{\partial f}{\partial x_2} + \Delta f - x_1^2\frac{\partial^2 f}{\partial x_1^2} - 2x_1x_2\frac{\partial^2 f}{\partial x_1 \partial x_2} - x_2^2\frac{\partial^2 f}{\partial x_2^2}\right).$$

At the two-dimensional North Pole $(x_1, x_2) = (0, 1)$ of the unit circle, the Cartesian form representation of Lf reduces to

$$Lf = \frac{\sigma^2}{2}\left(-\frac{\partial f}{\partial x_2} + \frac{\partial^2 f}{\partial x_1^2}\right). \tag{21}$$

This formula admits an intuitive and useful interpretation. The term $\frac{\sigma^2}{2}\frac{\partial^2 f}{\partial x_1^2}$ is the generator of a one-dimensional random walk in the horizontal direction. The term $-\frac{\sigma^2}{2}\frac{\partial f}{\partial x_2}$ is the generator of vertical displacements that project a Brownian particle moved along the tangent line back to the unit circle.

4.4. Brownian motion on a sphere

The generator for Brownian motion on the sphere $\mathbb{S}^{d-1}$, $d \geq 2$ can be constructed using a simple analogy with the random walk on the circle $\mathbb{S}^1$. In view of the above considerations, the expected form of the generator at the d-dimensional North Pole $(x_1, x_2, \ldots) = (0, 0, \ldots, 1)$ is

$$Lf = \frac{\sigma^2}{2}\sum_{i=1}^{d-1}\left(-\frac{\partial f}{\partial x_d} + \frac{\partial^2 f}{\partial x_i^2}\right) = \frac{\sigma^2}{2}\left(-(d-1)\frac{\partial f}{\partial x_d} + \Delta_{d-1} f\right), \tag{22}$$

where Δ_{d-1} is the Laplacian operator defined on the manifold of the first $d-1$ space directions. Since any Brownian motion is rotationally invariant, the complete Cartesian coordinate form of the generator reads

$$Lf = \frac{\sigma^2}{2}\left(-(d-1)\sum_{i=1}^{d} x_i\frac{\partial f}{\partial x_i} + \Delta f - \sum_{i,j=1}^{d} x_i x_j \frac{\partial^2 f}{\partial x_i \partial x_j}\right).$$

In the three-dimensional case $(d = 3)$, transformation of this differential operator to the spherical coordinates $0 \leq \theta \leq \pi$, $0 \leq \varphi < 2\pi$ yields

$$Lf = \frac{\sigma^2}{2}\left(\frac{1}{\sin\theta}\frac{\partial}{\partial\theta}\left(\sin\theta\frac{\partial f}{\partial\theta}\right) + \frac{1}{\sin^2\theta}\frac{\partial^2 f}{\partial\varphi^2}\right). \tag{23}$$

A rigorous derivation of this generator could be found, e.g., in Example 8.5.8 of [14].

5. Implementation of random walks

The reduced form (22) of the generator reveals that an infinitesimal Brownian motion on $\mathbb{S}^{d-1}$ is just the standard random walk on the $(d-1)$-dimensional tangential manifold, followed by a projection onto $\mathbb{S}^{d-1}$. In this section, we discuss practical approaches to implementation of random walks on $\mathbb{S}^{d-1}$. Some of them involve approximations that become exact as the time step Δt goes to zero. Exact random walks lead to more sophisticated numerical algorithms but allow the use of larger time steps than simplified approaches.

5.1. Standard random walk in $\mathbb{R}^d$ and on $\mathbb{S}^1$

The simplest distribution to implement numerically is the uniform one. We, therefore, start with approximating Brownian motion using Donsker's theorem and i.i.d. random numbers $X_{i,n}$ uniformly distributed on the interval $[-\frac{1}{2}, \frac{1}{2}]$. Multiplying each $X_{i,n}$ by the same scaling factor $\xi \in \mathbb{R}_+$, the mean squared displacement

$$\mathrm{Var}\big[\|X(t)\|^2\big] = \xi^2\mathbb{E}\left[\sum_{i=1}^{d}\left(\sum_{n=1}^{N} X_{i,n}\right)^2\right]$$

can be fitted to its deterministic counterpart $\sigma_d^2(t)$ defined by (18). We have

$$\mathbb{E}\left[\left(\sum_{n=1}^{N} X_{i,n}\right)^2\right] = \sum_{n=1}^{N}\mathbb{E}[X_{i,n}^2] + \sum_{n=1}^{N}\sum_{\substack{m=1\\ m\neq n}}^{N}\mathbb{E}[X_{i,n}X_{i,m}],$$

where $\mathbb{E}[X_{i,n}X_{i,m}] = \mathbb{E}[X_{i,n}]\mathbb{E}[X_{i,m}] = 0$ since the random numbers $X_{i,n}$ are independent with mean zero. The variance of the uniform distribution on $[-\frac{1}{2}, \frac{1}{2}]$ is

$$\mathbb{E}[X_{i,n}^2] = \int_{-1/2}^{1/2} x^2 dx = \frac{1}{12}.$$

It follows that:

$$\mathbb{E}\left[\left(\sum_{n=1}^{N} X_{i,n}\right)^2\right] = \mathbb{E}\left[\sum_{n=1}^{N} X_{i,n}^2\right] = \frac{N}{12} = \frac{t}{12\Delta t},$$

and, therefore, $\mathrm{Var}[\|X(t)\|^2] = \frac{d\xi^2 t}{12\Delta t}$. For this variance to coincide with $\sigma_d^2(t) = 2dDt$, the random numbers $X_{i,n}$ should be multiplied by

$$\xi = \sqrt{24D\Delta t}.$$

To simulate the standard Brownian motion on the circle $\mathbb{S}^1$, we recall that it is defined by $X(t) = (X_1(t), X_2(t)) = (\cos(\sigma B(t)), \sin(\sigma B(t)))$ and the polar coordinate form of its generator is simply $Lf = \frac{\sigma^2}{2}\frac{\partial^2 f}{\partial \varphi^2}$. Hence, a random walk on $\mathbb{S}^1$ can be implemented by adding random perturbations of the form $\Delta\varphi = \xi\Phi$ to the polar angle φ of the unperturbed orientation vector

$$\mathbf{p} = \begin{pmatrix} p_1 \\ p_2 \end{pmatrix} = \begin{pmatrix} \cos\varphi \\ \sin\varphi \end{pmatrix} \in \mathbb{S}^1.$$

As before, the scaling factor $\xi = \sqrt{24D\Delta t}$ should be used if Φ is generated using the mean-zero variance-one uniform distribution on $[-\frac{1}{2}, \frac{1}{2}]$.

After generating $\Delta\varphi$, the orientation vector $\mathbf{p}$ is to be updated by adding

$$\Delta\mathbf{p} = \begin{pmatrix} \Delta p_1 \\ \Delta p_2 \end{pmatrix} = \begin{pmatrix} \cos(\varphi + \Delta\varphi) - \cos\varphi \\ \sin(\varphi + \Delta\varphi) - \sin\varphi \end{pmatrix}.$$

This perturbation produces $\mathbf{p} + \Delta\mathbf{p} \in \mathbb{S}^1$ corresponding to the angle $\varphi + \Delta\varphi$.

5.2. Projected Cartesian random walks on $\mathbb{S}^1$ and $\mathbb{S}^2$

An alternative approach to generating a random walk on $\mathbb{S}^1$ is based on the Cartesian form representation (21) of the generator Lf. The calculation of the perturbation vector $\Delta\mathbf{p}$ involves two steps: random walk on the tangential vector and projection onto $\mathbb{S}^1$. The tangential vector is collinear to $\mathbf{p}^\perp = (-p_2, p_1)^T$. Therefore, an increment of a Cartesian random walk in the tangential direction is $\mathbf{p}^\perp \xi X$, where the random variable X is uniformly distributed on $[-\frac{1}{2}, \frac{1}{2}]$ and $\xi = \sqrt{24D\Delta t}$. Projecting onto $\mathbb{S}^1$, we obtain

$$\mathbf{p} + \Delta\mathbf{p} = \frac{\mathbf{p} + \mathbf{p}^\perp \xi X}{\|\mathbf{p} + \mathbf{p}^\perp \xi X\|}.$$

The perturbation vector can now be read off

$$\Delta\mathbf{p} = \begin{pmatrix} \Delta p_1 \\ \Delta p_2 \end{pmatrix} = \frac{1}{\sqrt{1 + \xi^2 X^2}} \begin{pmatrix} p_1 - p_2 \xi X \\ p_2 + p_1 \xi X \end{pmatrix} - \begin{pmatrix} p_1 \\ p_2 \end{pmatrix}.$$

In a similar vein, a random walk on the sphere $\mathbb{S}^2$ can be implemented as a two-dimensional Cartesian random walk on the tangential plane followed by a projection onto $\mathbb{S}^2$. An orthonormal basis for the plane tangential to $\mathbb{S}^2$ at $\mathbf{p} = (p_1, p_2, p_3)^T$ is given by

$$\hat{e}_1 = \frac{1}{\sqrt{p_1^2 + p_3^2}} \begin{pmatrix} p_3 \\ 0 \\ -p_1 \end{pmatrix}, \quad \hat{e}_2 = \frac{1}{\sqrt{p_1^2 + p_3^2}} \begin{pmatrix} -p_1 p_2 \\ -(p_1^2 + p_3^2) \\ p_2 p_3 \end{pmatrix}. \tag{24}$$

Changing to the polar coordinates, we define an increment of a random walk on the tangential plane as follows:

$$\big(\hat{e}_1 \cos(\pi\Phi) + \hat{e}_2 \sin(\pi\Phi)\big)\xi X,$$

where the random variables X and Φ are uniformly distributed on $[-\frac{1}{2}, \frac{1}{2}]$, and $\xi = \sqrt{48D\Delta t}$. Projecting onto $\mathbb{S}^2$, we obtain

$$\mathbf{p} + \Delta\mathbf{p} = \frac{\mathbf{p} + \big(\hat{e}_1 \cos(\pi\Phi) + \hat{e}_2 \sin(\pi\Phi)\big)\xi X}{\|\mathbf{p} + \big(\hat{e}_1 \cos(\pi\Phi) + \hat{e}_2 \sin(\pi\Phi)\big)\xi X\|}.$$

The perturbation vector can now be read off

$$\Delta\mathbf{p} = \begin{pmatrix} \Delta p_1 \\ \Delta p_2 \\ \Delta p_3 \end{pmatrix} = \frac{1}{\sqrt{1 + \xi^2 X^2}} \begin{pmatrix} p_1 + \frac{p_3 \cos(\pi\Phi) + p_1 p_2 \sin(\pi\Phi))}{\sqrt{p_1^2 + p_3^2}} \xi X \\ p_2 - \sin(\pi\Phi)\sqrt{p_1^2 + p_3^2}\,\xi X \\ p_3 - \frac{p_1 \cos(\pi\Phi) - p_2 p_3 \sin(\pi\Phi))}{\sqrt{p_1^2 + p_3^2}} \xi X \end{pmatrix} - \begin{pmatrix} p_1 \\ p_2 \\ p_3 \end{pmatrix}.$$

To avoid computation of the tangent plane, Brownian motion on $\mathbb{S}^{d-1}$ can also be approximated by the Cartesian random walk in $\mathbb{R}^d$ followed by an orthogonal projection onto $\mathbb{S}^{d-1}$. In the case $d = 3$, this projection-based random walk approach yields the perturbation vector

$$\Delta\mathbf{p} = \begin{pmatrix}\Delta p_1\\ \Delta p_2\\ \Delta p_3\end{pmatrix} = \frac{1}{\sqrt{\sum_{i=1}^3 (p_i+\xi X_i)^2}}\begin{pmatrix}p_1+\xi X_1\\ p_2+\xi X_2\\ p_3+\xi X_3\end{pmatrix} - \begin{pmatrix}p_1\\ p_2\\ p_3\end{pmatrix},$$

where the i.i.d random variables X_i, $i = 1, 2, 3$ are uniformly distributed on $[-\frac{1}{2}, \frac{1}{2}]$, and $\xi = \sqrt{24D\Delta t}$. Moosaie and Manhart [6] used this random walk approach for Monte Carlo simulations of turbulent drag reduction in fiber suspension flows.

In order to prove rigorously that these random walks converge to the Brownian motion on the sphere, one can follow the steps of the proof of Donsker's theorem. More precisely, one needs to check that the corresponding finite-dimensional distributions of these random walks converge as $\Delta t \to 0$, and then prove tightness of the family of probability measures induced by these random walks. We do not elaborate on these arguments here.

5.3. CDF-fitted spherical random walk on $\mathbb{S}^2$

In simulations of a Brownian motion on $\mathbb{R}^d$, it is worthwhile to replace the uniform distribution of the increments of the random walk with a normal distribution. The main benefit of this approach lies in the fact that the random walk has the exactly the same distribution as a Brownian motion for times $n\Delta t$. Therefore, accurate computations can be performed with relatively large Δt. Similarly, we can define a random walk on $\mathbb{S}^2$. More specifically, suppose that the random variable $\hat{X}_3$ represents the vertical coordinate of the Brownian motion on a sphere in the rotated frame at $t = \Delta t$. The corresponding probability density distribution is given by (9). Using the tangential basis vectors $\hat{e}_1$ and $\hat{e}_2$ defined by (24), we update the orientation vector $\mathbf{p} = (p_1, p_2, p_3)^T$ by adding perturbations of the form

$$\Delta\mathbf{p} = (\hat{X}_3 - 1)\mathbf{p} + \sqrt{1+\hat{X}_3^2}\big(\hat{e}_1\cos(2\pi\,\Phi) + \hat{e}_2\sin(2\pi\,\Phi)\big), \tag{25}$$

where the random variable Φ is uniformly distributed on $[-\frac{1}{2}, \frac{1}{2}]$.

Let $F_\tau(x) = \mathbb{P}(\hat{X}_3 \le x)$, $x \in [-1, 1]$, $\tau = D\Delta t$ denote the cumulative distribution function (CDF). By (9) we have

$$F_\tau(x) = \sum_{n=0}^{\infty}\frac{2n+1}{2}\int_{-1}^{x} P_n(y)dy. \tag{26}$$

Since

$$\int_{-1}^{x} P_n(y)dy = \frac{1}{2n+1}(P_{n+1}(x) - P_{n-1}(x)), \qquad P_{-1} \equiv 0,$$

formula (26) also could be rewritten as

$$F_\tau(x) = \frac{x}{2} + \frac{1}{2}\sum_{n=1}^{\infty}\exp\left(-n(n+1)\tau\right)(P_{n+1}(x) - P_{n-1}(x)). \tag{27}$$

Then $\hat{X}_3$ can be simulated numerically as

$$\hat{X}_3 = F_\tau^{-1}(U), \tag{28}$$

where U is uniformly distributed on [0,1]. Unfortunately, the CDF defined by (26) cannot be easily inverted to transform $U \in [0, 1]$ into $\hat{X}_3$ defined by (28). Using approximation (10), Chen and Yu [8] replaced $F_\tau(x)$ by

$$\tilde{F}_\tau(x) = \exp\left(-\frac{\arccos^2 x}{4\tau}\right). \tag{29}$$

The resulting closed-form expression for $\hat{X}_3$ reads

$$\hat{X}_3 = \cos(\sqrt{-4\tau\ln(U)}). \tag{30}$$

Since the derivation of (10) is based on the assumption that $\tau \ll 1$, the cumulative probability $\tilde{F}_\tau(x)$ may become a poor approximation to $F_\tau(x)$ defined by (26) as τ increases. Accurate results can only be expected for $\tau \le 0.1$ (see Fig. 3 in [8]). To avoid large modeling errors, the approximate CDF formula (30) should not be used for $\tau > 1$.

As an alternative to approximating $F_\tau(x)$ by $\tilde{F}_\tau(x)$, we calculate the cumulative probabilities $F_j = F_\tau(x_j)$, $x_j = j/M$ for $j = -M, \ldots, M$ *off-line* and store the results in a *look-up table*. Since F_τ is continuous and increasing on $[-1, 1]$, it attains each intermediate value. It follows that for any $U \in [0, 1]$ there exists an index j such $U \in \left[F_{j-1}, F_j\right]$. Let $F_\tau^j(x)$ be the linear interpolant of F_{j-1} and F_j, i.e.,

$$F_\tau^j(x) = F_{j-1}\frac{x_j - x}{\Delta x} + F_j\frac{x - x_{j-1}}{\Delta x}, \quad x \in [x_{j-1}, x_j], \quad \Delta x = \frac{1}{M}.$$

Then $(F_\tau^j)^{-1} : [F_{j-1}, F_j] \to [x_{j-1}, x_j]$ is linear too and can be used to calculate

$$\hat{X}_3 = (F_\tau^j)^{-1}(U) = x_{j-1}\frac{F_j - U}{F_j - F_{j-1}} + x_j\frac{U - F_{j-1}}{F_j - F_{j-1}}$$

for our spherical random walk approach based on the use of look-up tables.

Note that if τ is large enough so that the sum in (27) is negligible and, therefore,

$$F_\tau(x) \approx \frac{x}{2},$$

then, by the Archimedean projection property, the new position of the particle is uniformly distributed on a sphere and we do not need any formulas to simulate it - just pick a new position at random with uniform distribution on the sphere.

6. Case study: orientation tensors

In this section, we compare and evaluate different random walk approaches to Monte Carlo simulation of fiber orientation dynamics. The probability density distribution $f : \mathbb{S}^{d-1} \to \mathbb{R}^+$ can be reconstructed from instantaneous orientations $\mathbf{p}_m$ of N_f evolving Brownian fibers using (14) or the representation of $f(\mathbf{p}, t)$ in terms of orientation tensors [15]. In practical applications, the effective stress of a semi-dilute fiber suspension depends on the orientation tensors corresponding to the second and fourth-order moments

$$\mathbf{A}(t) = \int_{\mathbb{S}^{d-1}} \mathbf{p}\otimes\mathbf{p}\ f(\mathbf{p},t)\,\mathrm{d}\mathbf{p} = \left\{A_{ij}\right\}_{i,j=1}^{d}, \tag{31}$$

$$\mathbb{A}(t) = \int_{\mathbb{S}^{d-1}} \mathbf{p}\otimes\mathbf{p}\otimes\mathbf{p}\otimes\mathbf{p}\ f(\mathbf{p},t)\,\mathrm{d}\mathbf{p} = \left\{A_{ijkl}\right\}_{i,j,k,l=1}^{d} \tag{32}$$

which provide sufficient information for rheological modeling purposes.

Substituting reconstruction (14) into (31) and (32), we obtain

$$\mathbf{A} = \frac{1}{N_f}\sum_{m=1}^{N_f} \mathbf{p}_m\otimes\mathbf{p}_m, \tag{33}$$

$$\mathbb{A} = \frac{1}{N_f}\sum_{m=1}^{N_f} \mathbf{p}_m\otimes\mathbf{p}_m\otimes\mathbf{p}_m\otimes\mathbf{p}_m, \tag{34}$$

where N_f is the number of evolved fibers. Remarkably, the so-defined tensors $\mathbf{A}$ and $\mathbb{A}$ can be calculated without reconstructing f.

The following abbreviations are used for the methods under investigation:

- RW-CP: Cartesian random walk in $\mathbb{R}^3$ + projection onto $\mathbb{S}^2$ (Section 5.2);
- RW-TP: Random walk on the tangential plane + projection onto $\mathbb{S}^2$ (Section 5.2);
- RW-VH: Random walk in the vertical direction + random walk on the horizontal plane (Section 5.3).

An additional letter X$\in${A,E} is used in abbreviations of the form RW-VH-X to distinguish between two different implementations:

- RW-VH-A: Approximate random walk method of Chen and Yu [8];
- RW-VH-E: Exact random walk using look-up tables for the CDF.

Numerical studies of the above methods are performed for the three-dimensional spherical heat equation (1). In the first set of numerical experiments, the initial condition is the δ distribution (5) corresponding to

$$\mathbf{p}_0 = (0, 0, 1)^T.$$

The components of exact orientation tensors are given by

$$A_{ij}(t) = \int_0^{2\pi}\int_0^{\pi} p_i(\theta,\varphi)p_j(\theta,\varphi)f(\cos\theta,t)\sin\theta\,d\theta d\varphi, \tag{35}$$

$$A_{ijkl}(t) = \int_0^{2\pi}\int_0^{\pi} p_i(\theta,\varphi)p_j(\theta,\varphi)p_k(\theta,\varphi)p_l(\theta,\varphi)f(\cos\theta,t)\sin\theta\,d\theta d\varphi, \tag{36}$$

where $f(\hat{x}_3, t)$ is the azimuthal probability distribution defined by (9). The above integrals can be further simplified by making an appropriate change of variables. For example, A_{33} written in terms of $u = \cos\theta$ becomes

$$A_{33}(t) = 2\pi\int_{-1}^{1} u^2 g(u,t)du, \tag{37}$$

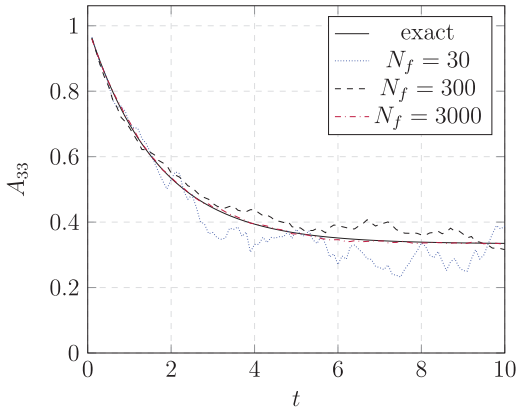

Fig. 2. Dependence of the RW-CP results for A_{33} on the number of particles. Test problem: spherical heat equation with the initial condition given by the δ distribution.

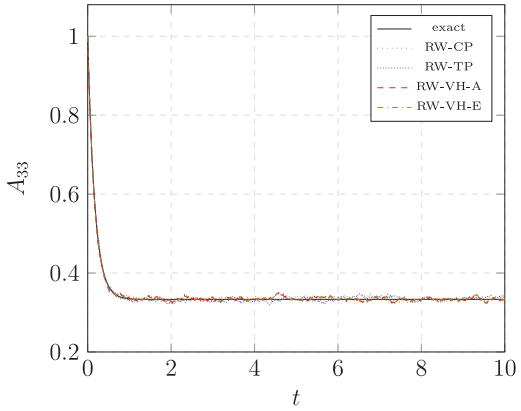

Fig. 3. Evolution of A_{33} in random walks using $\tau = 0.01$ vs. the exact solution. Test problem: spherical heat equation with the initial condition given by the δ distribution.

where

$$g(u,t) = \frac{1}{4\pi}\sum_{n=0}^{m}(2n+1)\exp[-n(n+1)Dt]P_n(u). \tag{38}$$

The number of terms in the truncated series approximations to $f(\theta, t)$ must be chosen sufficiently large to obtain the exact value of the given tensor component. In fact, orientation tensors of any order are uniquely defined by the first coefficients c_j of the truncated sum approximation (12) by a linear combination of spherical harmonics ψ_j. Hence, the exact values of A_{ij} and A_{ijkl} can be calculated using a small number m of terms in (38). More terms are generally required to calculate higher-order orientation tensors exactly.

To obtain a good approximation of orientation tensors in Monte Carlo simulations leading to (33) and (34), the number N_f of particles to be evolved must be chosen sufficiently large. Fig. 2 illustrates the influence of the number of particles on the accuracy of numerical results. It can be seen that as many as 3000 particles may be required to capture the evolution of A_{33} with high precision. The results obtained with other approaches exhibit similar dependence on the number of particles. In the remaining numerical experiments of this section, we perform random walks with 4000 particles.

The approximations to A_{33} presented in Figs. 3 and 4 indicate that all random walk methods under consideration produce similar results for small values of the scaled time step $\tau = D\Delta t$. Fig. 5 demonstrates that our exact random walk (RW-VH-E) outperforms RW-CP and RW-TP as the time step increases and the accuracy of projection-based methods deteriorates.

For further comparison of different methods, we perform Monte Carlo simulations for a randomly chosen initial state. In this set of experiments, the orientation angles of sample fibers at $t = 0$ are defined by

$$\Theta = \frac{\pi}{6}U, \quad \Phi = 2\pi U,$$

where U is a random variable uniformly distributed on [0,1]. This variable is generated using an identical seed for all methods. For each method, we present the results obtained with three different time steps. Since no exact solution is available for the case of random initial data, the results corresponding to $\tau = 0.01$ serve as reference solutions for each method.

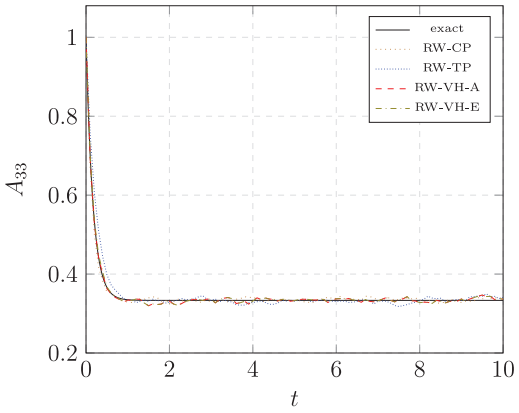

Fig. 4. Evolution of A_{33} in random walks using $\tau = 0.1$ vs. the exact solution. Test problem: spherical heat equation with the initial condition given by the δ distribution.

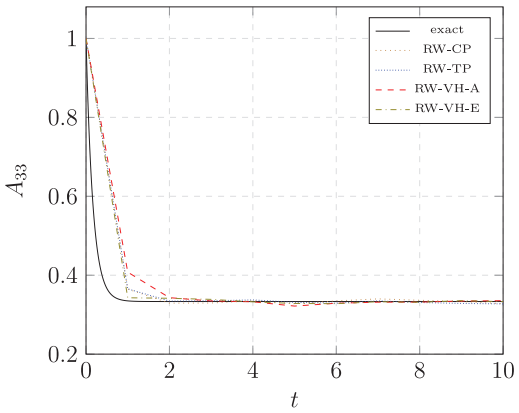

Fig. 5. Evolution of A_{33} in random walks using $\tau = 1.0$ vs. the exact solution. Test problem: spherical heat equation with the initial condition given by the δ distribution.

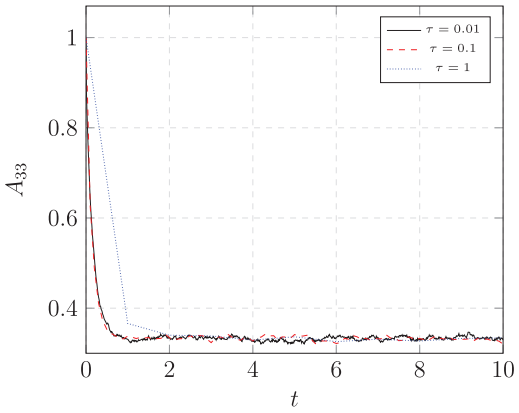

Fig. 6. Evolution of A_{33} in random walks using RW-CP. Test problem: spherical heat equation with the random initial condition.

Indeed, this value of τ was found to produce sufficiently accurate approximations to the known exact solution of the first test problem (see Fig. 3).

The numerical approximations to the component A_{33} of the second-order orientation tensor are shown in Figs. 6–9. Note that the RW-VH-E solution obtained with $\tau = 1$ is as accurate as the reference solution throughout the simulation run, whereas other methods produce significant errors after the first large time step. As in the first test, all methods yield accurate predictions for the constant value of A_{33} to which the reference solution converges as time goes. Clearly, individual components of low-order orientation tensors provide limited information about the probability distribution. As another

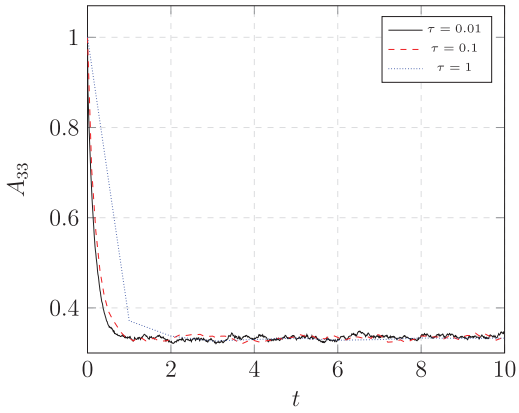

Fig. 7. Evolution of A_{33} in random walks using RW-TP. Test problem: spherical heat equation with the random initial condition.

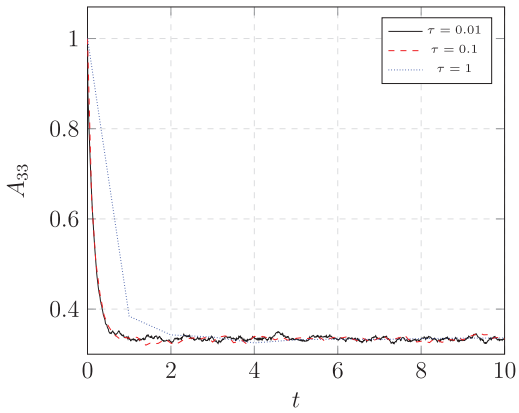

Fig. 8. Evolution of A_{33} in random walks using RW-VH-A. Test problem: spherical heat equation with the random initial condition.

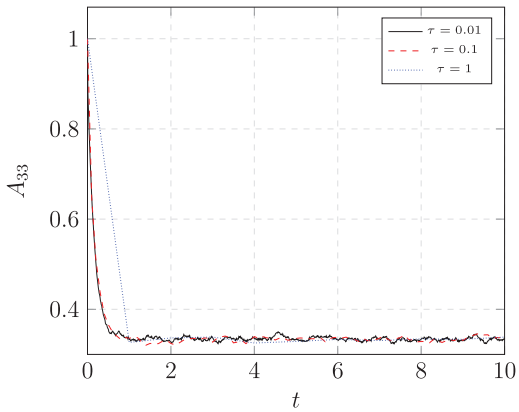

Fig. 9. Evolution of A_{33} in random walks using RW-VH-E. Test problem: spherical heat equation with the random initial condition.

quantity of interest, we consider the mean-squared angular displacement

$$\mathrm{MSD}(t) = \frac{1}{N_f}\sum_{m=1}^{N_f}(\theta_m(t) - \theta_m(0))^2,$$

where N_f is the number of samples. The evolution of MSD for the two versions of RW-VH is shown in Figs. 10 and 11. The RW-VH-A method produces a significant overshoot after the first time step corresponding to $\tau = 1$. The random walk approach using the look-up table (RW-VH-E) is seen to produce excellent results for all three values of τ already at early

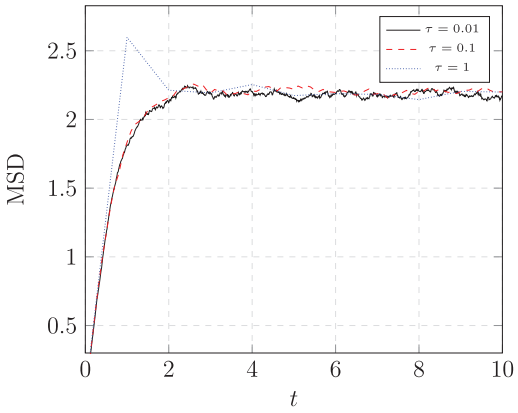

Fig. 10. Evolution of MSD in random walks using RW-VH-A. Test problem: spherical heat equation with the random initial condition.

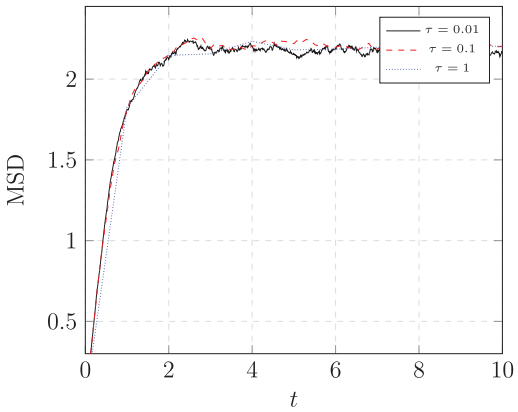

Fig. 11. Evolution of MSD in random walks using RW-VH-E. Test problem: spherical heat equation with the random initial condition.

stages. We conclude that it is better suited for simulating dynamic changes of orientation states with large time steps than any other method considered in this study.

7. Conclusions

It is hoped that the presented analysis of spherical Brownian motions gives additional insights into their mathematical properties and numerical behavior of random walk methods for Monte Carlo simulations. Clearly, the random walk methodology is not restricted to simulations of pure Brownian diffusion. It can readily be extended to Lagrangian models of orientation dynamics in which moving fibers may also be advected or rotated by deterministic velocity fields. The presented methodology is currently being used to simulate Brownian diffusion effects in non-Newtonian models of fiber suspension flows. Simulation results for the 3D axisymmetric contraction benchmark and numerical studies of closure approximations will be presented elsewhere.

Acknowledgments

The work of Omid Ahmadi and Dmitri Kuzmin was supported by the German Research Association (DFG) under grant KU 1530/13-1. The work of Alexei Novikov was supported by the US NSF grants DMS-1515187 and DMS-1813943.

Supplementary material

Supplementary material associated with this article can be found, in the online version, at doi:10.1016/j.amc.2019.124670.

References

[1] S. Montgomery-Smith, D. Jack, D.E. Smith, The fast exact closure for Jefferys equation with diffusion, J. Non-Newton. Fluid Mech. 166 (2011) 343–353.
[2] F. Folgar, C.L. Tucker, Orientation behavior of fibers in concentrated suspensions, J. Reinf. Plast. Compos. 3 (2) (1984) 98–119.

[3] G.B. Jeffery, The motion of ellipsoidal particles immersed in a viscous fluid, Proc. Royal Soc. Lond. A: Math. Phys. Eng. Sci. 102 (715) (1922) 161–179, doi:10.1098/rspa.1922.0078.
[4] K. Chiba, F. Chinesta, Numerical simulation of flow kinematics and fiber orientation for multi-disperse suspension, Rheol. Acta 45 (1) (2005) 1–13, doi:10.1007/s00397-004-0431-2.
[5] J.J.J. Gillissen, B.J. Boersma, P.H. Mortensen, H.I. Andersson, The stress generated by non-Brownian fibers in turbulent channel flow simulations, Phys. Fluids 19 (11) (2007).
[6] A. Moosaie, M. Manhart, Direct Monte Carlo simulation of turbulent drag reduction by rigid fibers in a channel flow, Acta Mech. 224 (2013) 2385–2413.
[7] A. Sokolichin, G. Eigenberger, A. Lapin, A. Lübbert, Dynamic numerical simulation of gas-liquid two-phase flows Euler/Euler versus Euler/Lagrange, Chem. Eng. Sci. 52 (4) (1997) 611–626.
[8] Y.K. Chen, C.P. Yu, Monte Carlo simulation of fiber orientation in a shear flow with Brownian rotation, Aerosol Sci. Technol. 16 (4) (1992) 255–264.
[9] V. Tulovsky, L. Papiez, Formula for the fundamental solution of the heat equation on the sphere, Appl. Math. Lett. 14 (2001) 881–884.
[10] D. Knezevic, Finite element methods for deterministic simulation of polymeric fluids, Technical Report, NA-06/19, Oxford University Computing Laboratory, 2006. Numerical Analysis Group.
[11] D. Knezevic, E. Süli, A heterogeneous alternating-direction method for a micro-macro dilute polymeric fluid model, M2AN 43 (2009) 1117–1156.
[12] T. Carlsson, T. Ekholm, C. Elvingson, Algorithm for generating a Brownian motion on a sphere, J. Phys. A: Math. Theor. 43 (50) (2010).
[13] J. Nissfolk, T. Ekholm, C. Elvingson, Brownian dynamics simulations on a hypersphere in 4-space, J. Chem. Phys. 119 (13) (2003) 6423–6432.
[14] B. Oksendal, Stochastic Differential Equations: An Introduction With Applications, Universitext, 6th edition, Springer-Verlag, Berlin, 2003, doi:10.1007/978-3-642-14394-6.
[15] D.A. Jack, D.E. Smith, Assessing the use of tensor closure methods with orientation distribution reconstruction functions, J. Compos. Mater. 38 (21) (2004) 1851–1871.